

## 13C.5 Influence of cloud-radiative feedback on tropical cyclone motion: Symmetric contributions

Robert G. Fovell<sup>1\*</sup>, Kristen L. Corbosiero<sup>1</sup> and Hung-Chi Kuo<sup>2</sup>

<sup>1</sup>University of California, Los Angeles, California, USA

<sup>2</sup>National Taiwan University, Taipei, Taiwan

### 1. Introduction

Cloud microphysical parameterizations (MPs) contain a large number of assumptions and approximations related to particle fallspeeds, size distributions and conversion rates, and thus even ostensibly similar schemes can produce significantly different concentrations and species apportionments of hydrometeors. This can have a direct and material impact on tropical cyclone (TC) motion, as demonstrated by Fovell et al. (2009; hereafter P1). That study employed a specially modified version of the real-data WRF-ARW having a large land-free domain with uniform and fixed sea-surface temperatures and initialized with a calm, horizontally homogeneous environment following Jordan (1958). Triple nesting was used with horizontal grid spacings down to 3 km.

Three MPs were examined in P1: Kessler (K), LFO (L) and WSM3 (W). They showed that microphysics modulates the tangential wind strength in the outer portion of the model storms, well beyond the core, winds are known to influence vortex self-propagation owing to the “beta drift” (e.g., Fiorino and Elsberry 1989; hereafter FE). In the absence of strong environmental flow, the microphysics-modulated drift alone could produce substantial differences among cyclone position forecasts within a single day in this realistically curved-Earth framework.

Recently, Fovell et al. (2010; hereafter P2) updated the P1 experiment to include versions of Seifert and Beheng’s (2006) dual-moment MP and investigated the role of cloud-radiative feedback (CRF) on vortex motion. CRF involves the processes by which condensation particles influence the absorption and emission of longwave (LW) and shortwave (SW) radiation. When CRF is active (the default situation), a range of tracks similar to P1 was obtained (Fig. 1a). Based on the final 24 h average motion, the tracks labeled S<sub>2</sub> and W, representing the most and least sophisticated ice-containing MPs, were diverging at roughly 150 km per day.

However, this track variation *nearly vanished* when CRF was deactivated (Fig. 1b). Although P2 demonstrated that storm asymmetries were also significant, herein we focus on the role of CRF in altering the symmetric component of storm structure, extending P1’s analysis. Analyses will make use of vortex-following composites averaged over the final 24 h, focusing on the azimuthally symmetric components.

### 2. Symmetric distributions of diabatic heating and cooling

The CRF sensitivity emerges because schemes tend to produce different amounts of condensate species that have significantly disparate radiative impacts when CRF is active. Radiative influence largely responds to assumed or calculated particle cross-sectional areas. As an example, the L scheme has a swift evolutionary path to compact graupel particles (Fig. 2) typically assumed to have negligible radiative forcing. In contrast, Seifert-Beheng version S<sub>2</sub> supported considerably more cloud ice that contributes significantly to LW absorption. From an observational standpoint, it is very difficult to judge which is more realistic, but the consequences of these arguable microphysical assumptions are not small.

These storms also varied with respect to total condensation produced as well as amounts and distributions of diabatic heating and cooling due to microphysics and radiation (Fig. 3). It is clear that S<sub>2</sub> had more radially extensive diabatic heating, especially compared to the CRF-off run L\*. This is consistent with its wider anvil (Fig. 4), which itself induced a more pronounced radiative impact characterized by net cooling at cloud top and weak warming farther below. Storm S<sub>2</sub> also possessed the strongest upper tropospheric radial outflow of the trio (Fig. 4), which can serve to transport radiatively active particles farther outward. We argue below that there may be a synergistic relationship at work here.

The more extensive heating coincided with stronger lower tropospheric tangential winds (Fig. 5). These winds advect planetary vorticity and establish the *beta gyres* (Holland 1983; Chan and Williams 1987) that impart motion on vortices in otherwise qui-

---

\*Corresponding author address: Prof. Robert Fovell, UCLA Atmospheric and Oceanic Sciences, Los Angeles, CA 90095-1565. E-mail: rfovell@ucla.edu.

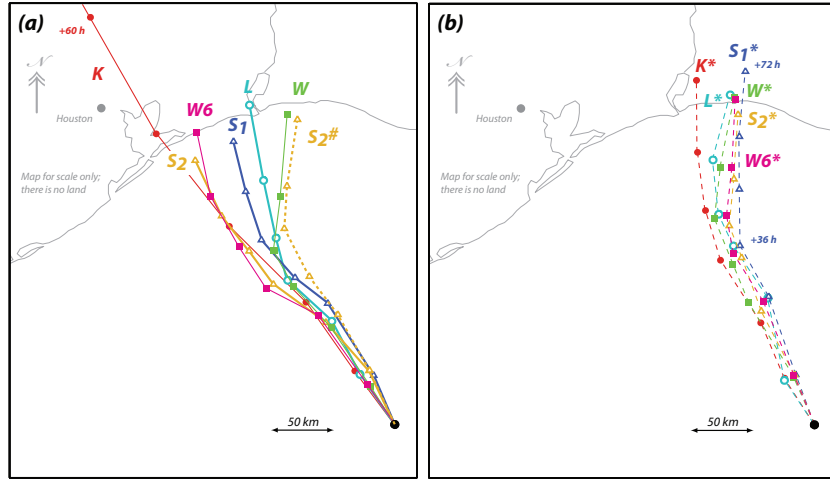


Fig. 1: Twelve hourly positions over 72 h for storms using Kessler (K), LFO (L), WSM3 (W), WSM6 (W6), and Seifert-Beheng ( $S_1$ ,  $S_2$ ,  $S_2^\#$ ) schemes with CRF (a) on and (b) off. Asterisk indicates CRF off;  $S_2^\#$  treats cloud ice as snow for radiative calculations. The 72 h K position is beyond the subdomain depicted. U.S. Gulf Coast segment included for scale; the model has no land. After Fovell et al. (2010), Figs. 1 and 4.

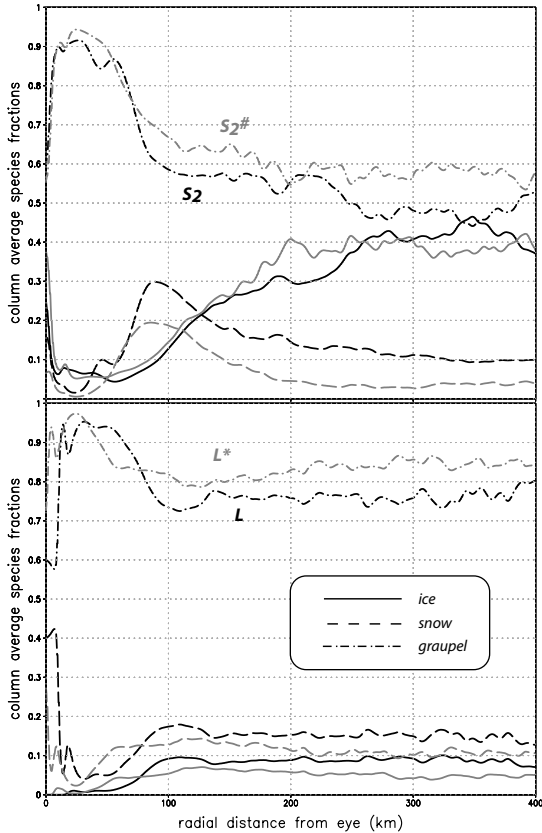


Fig. 2: Ice species fractions vs. radial distance, computed using symmetric components from vortex-following composites, for simulations using versions of the L and  $S_2$  MPs.  $L^*$  ignores CRF;  $S_2^\#$  treats cloud ice as snow for radiative calculations.

escent environments. Generally, stronger winds at large radius ( $r > 300$  km or so) results in progres-

sively faster and more northwestward translation, consistent with FE. While the CRF-active runs exhibit variation with respect to the outer winds (e.g., Fig. 5 a,b) that among the CRF-off storms (typified by Fig. 5c) was quite small.

### 3. Further idealized experiments with heat sources and sinks

Altering microphysical assumptions clearly changes the spatial patterns of diabatic heating from phase changes as well as radiative forcing that can differentially impact storm structure and motion. This is demonstrated using externally specified, spatially confined heat sources that resemble those appearing at outer radii in the simulated hurricanes, using the Rotunno and Emanuel (1987; hereafter RE) axisymmetric model with 5 km radial and 1.25 km vertical grid spacings and the Coriolis parameter,  $f$ , set for  $20^\circ\text{N}$ . The simulations employ RE’s “mixed” Jordan sounding, but moisture and the initial vortex have been removed. Friction, subgrid mixing, the surface sensible heat flux and and Newtonian damping representing background radiative cooling are still active because the goal is to assess how a model that produces reasonable hurricane structures responds to diabatic sources and sinks of various shapes and sizes. This effort is complementary to more simplified and theoretical treatments of heat and momentum sources (e.g., Willoughby 1979; Shapiro and Willoughby 1982; Schubert and Hack 1982; Holland and Merrill 1984, etc.).

As an example, the response to a elliptically shaped heat source centered at  $(r,z) = (100, 5)$  km is shown in Fig. 6. The source’s horizontal and vertical radii

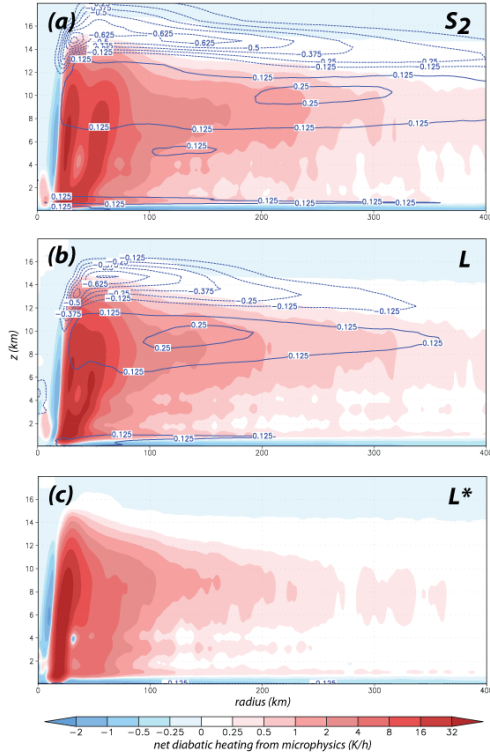


Fig. 3: Radius-height cross-sections of net diabatic heating from microphysics (shaded as shown) and radiation (0.125 K/h contours) for  $S_2$ ,  $L$  and  $L^*$ , representing the azimuthally symmetric components extracted from vortex-following composites constructed over the final 24 h. The background atmospheric cooling rate is removed from the latter.

are 25 and 3 km, respectively, and the  $1.8 \text{ K h}^{-1}$  maximum magnitude was suggested by Fig. 3. As expected from past studies, the temperature and pressure responses (Figs. 6a, b) are primarily concentrated between the heat source and the central axis. Horizontal velocity directed radially outward (inward) is produced above (below) the source on its outer side. Cyclonic flow is induced just behind and beneath the source, extending to the surface. Thus, a midtropospheric heat source serves to strengthen the tangential winds at larger radius that are advecting planetary vorticity and establishing the beta gyres. The source also enhances the anticyclonic flow in the upper troposphere even farther outward.

Replacing the original source with a sink is nearly tantamount to reflecting this response about a horizontal axis (not shown), indicating that evaporation and melting well beyond the core can reduce the outer wind strength. Somewhat surprisingly, shifting the heat source location inward or outward has relatively little effect (Figs. 7a,b) but the reduced lower tropospheric response resulting from elevating the source (Fig. 7c) could be easily anticipated. Widening the source magnifies its impact on the tangential winds substantially (Fig. 8).

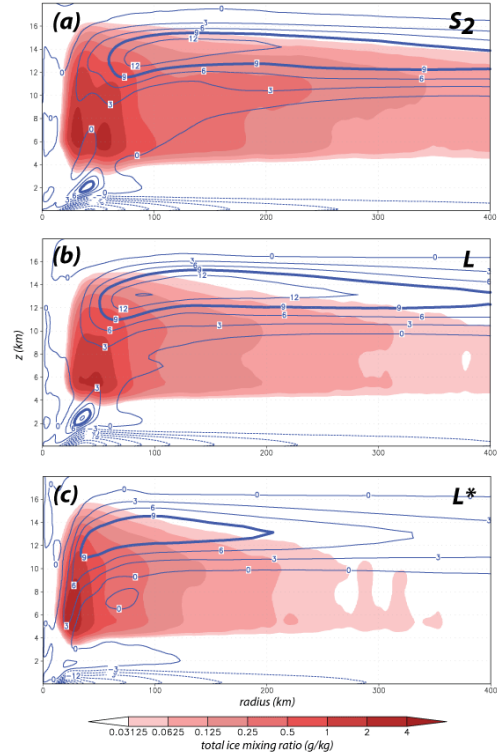


Fig. 4: As in Fig. 3 but showing total ice content (shaded) and radial wind (3 m/s contours, 9 m/s highlighted).

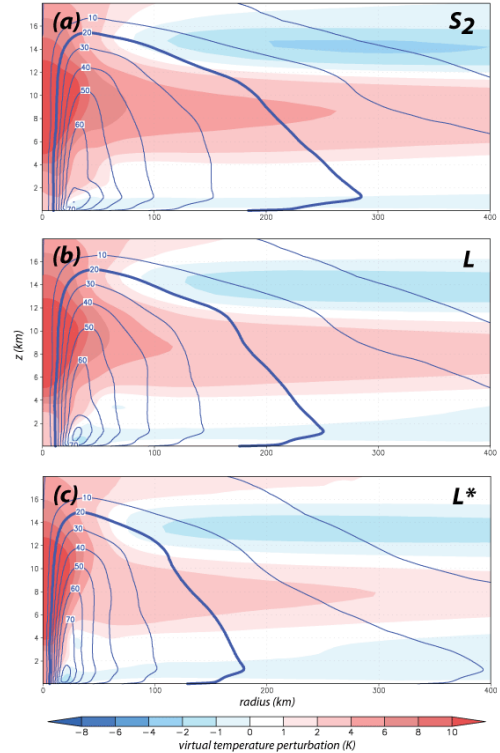


Fig. 5: As in Fig. 3, but showing virtual temperature perturbation from initial state (shaded) and tangential wind (10 m/s contours, 20 m/s contour highlighted).

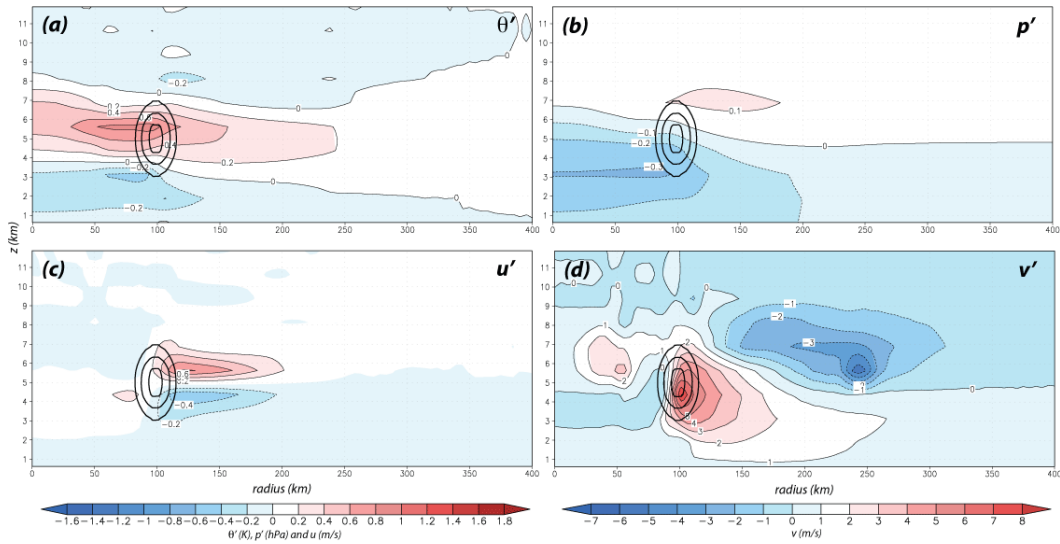


Fig. 6: RE model response to maintained heat source (thick 0.5 K/h contours): (a) potential temperature perturbation; (b) pressure perturbation; (c) radial velocity; (d) tangential velocity, all contoured/shaded as indicated.

Taken together, these simple experiments indicate that MP schemes producing more radially extensive diabatic heating, especially when extended to the lower troposphere, can induce stronger cyclonic winds at larger radii. This is consistent with Wang (2009), who cited heating in the outer rainbands as a principal factor influencing the azimuthally symmetric structure of TCs, and probably explains why the Kessler (K) MP possessed such strong winds leading to relatively rapid translation in P1 and P2. With CRF active, K exhibited extensive midtropospheric heating (Fig. 9a). However, the heating was weaker, less extensive and also located higher up when CRF was neglected (Fig. 9b), which resulted in diminished tangential flow and strongly suggests that cloud-radiative feedback plays an important role in determining the heating structure despite being relatively small in magnitude.

#### 4. Anvil self-spreading and concluding remarks

The primary role of CRF may be to encourage radial anvil expansion. In these simulations, the radiative forcing has a dipole structure consisting of warming shifted somewhat outward and downward relative to the cloud top cooling, with radial outflow located in between. Figure 10’s top panel illustrates this for the L case and the bottom panel depicts the radial wind response to a similarly situated sink/source pair in the RE model. The principal response is to establish flow directed away from the storm center. Although ostensibly weak in magnitude, the outflow is persistent because the radiative forcing is dominated by LW and thus less subject to diurnal variation. This was demonstrated via simulations in which only the SW component of CRF was deactivated; the model hurricanes exhibited little change (not shown).

This may be an example of what Krueger and Zulauf (2005; hereafter KF) termed “mesoscale radiatively-induced anvil spreading” or MRAS. In idealized simulations in a non-rotating reference frame, KF demonstrated a spread rate of  $1.2 \text{ m s}^{-1}$ , which is about 100 km per day if maintained at that rate. In the TC context, the radial outflow is transporting hydrometeors that carry the radiative forcing. That forcing helps support and extend the outflow farther, helping push condensate particles farther outward and thus radially extending the radiative forcing, a weak positive feedback depicted schematically in Fig. 11. More efficient outward transport of hydrometeors may serve to actively moisten the atmosphere at larger and larger radius, rendering it more conducive to convection. With that convection comes latent heating, which helps strengthen the tangential winds that influence the track.

An inescapable conclusion is that microphysics is important, and owing to CRF and differential radiative impact it matters if a scheme tends to produce relatively more of one hydrometeor species than another. We reiterate that only symmetric contributions to vortex structure and motion have been considered herein and that asymmetric contributions from convection are not negligible (e.g., Fovell et al. 2010). It is stipulated that calibration and validation of the diabatic effects of microphysics and radiation, as well as further assessment of how they are treated in numerical models, is indicated.

#### 5. References

- Chan, J. C.-L., and R. T. Williams, 1987: Analytical and numerical studies of the beta-effect in tropical cyclone motion. *J. Atmos. Sci.*, **44**, 1257–1265.
- Fiorino, M. J., and R. L. Elsberry, 1989: Some aspects of vortex structure related to tropical cyclone

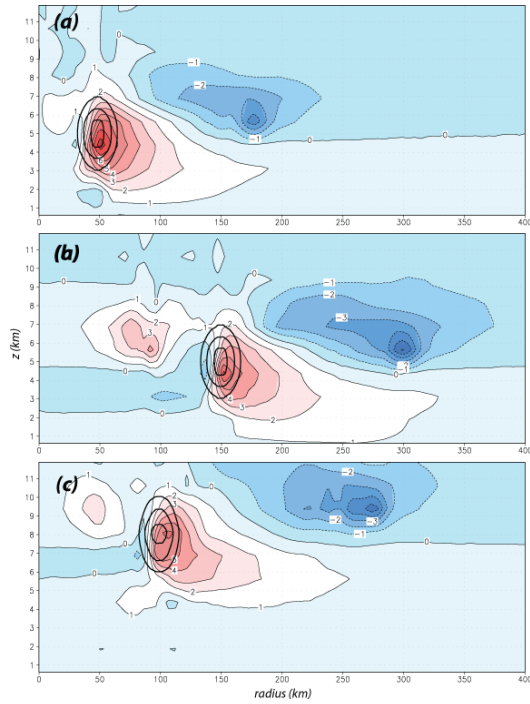


Fig. 7: As in Fig. 6d, but for sources moved: (a) inward; (b) outward; and (c) upward.

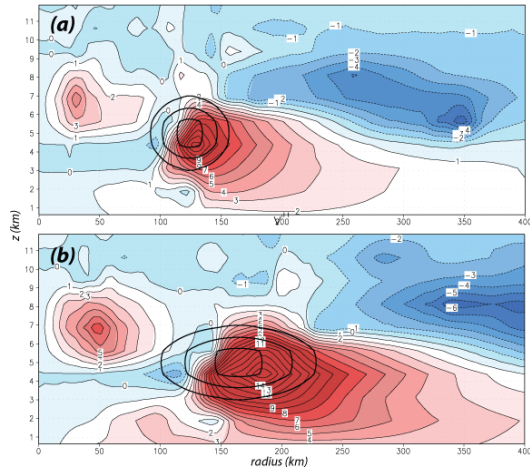


Fig. 8: As in Fig. 6d but for sources of different widths.

motion. *J. Atmos. Sci.*, **46**, 975–990.

Fovell, R. G., K. L. Corbosiero, and H.C. Kuo, 2009: Cloud microphysics impact on hurricane track as revealed in idealized experiments. *J. Atmos. Sci.*, **66**, 1764–1778.

Fovell, R. G., K. L. Corbosiero, A. Seifert, and K.-N. Liou, 2010): Impact of cloud-radiative processes on hurricane track. *Geoph. Res. Lett.*, **37**, L07808, doi:10.1029/2010GL042691.

Holland, G. J., 1983: Tropical cyclone motion: Environmental interaction plus a beta effect. *J. Atmos. Sci.*, **40**, 328–342.

Holland, G. J. and R. T. Merrill, 1984: On the dynamics of tropical cyclone structural changes. *Quart. J. Roy. Meteor. Soc.*, **110**, 723–745.

Jordan, C. L., 1958: Mean soundings for the West Indies area. *J. Meteor.*, **15**, 91–97.

Krueger, S. K., and M. A. Zulauf, 2005:

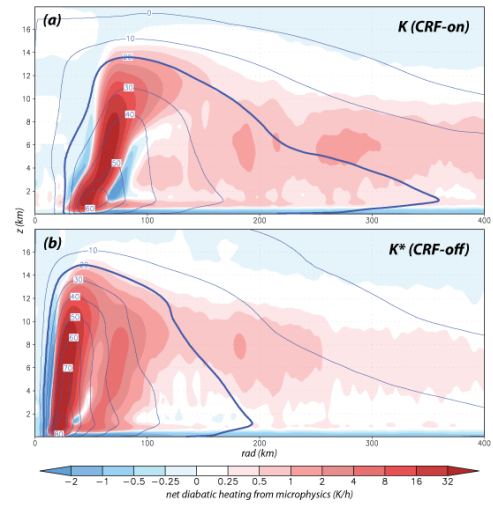


Fig. 9: Symmetric components of diabatic heating from microphysics (shaded) and tangential winds (10 m/s contours, 20 m/s contour highlighted) for Kessler (K) storms (a) with, and (b) without CRF.

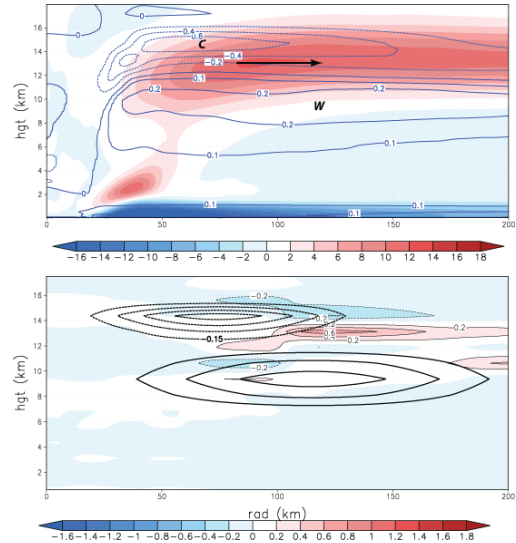


Fig. 10: Radial velocity (shaded) and diabatic sink/source from: (a) case L, representing diabatic radiative forcing; and (b) response of RE model to similar diabatic forcing. Diabatic sink (source) contour interval 0.2 (0.05) K/h in both panels.

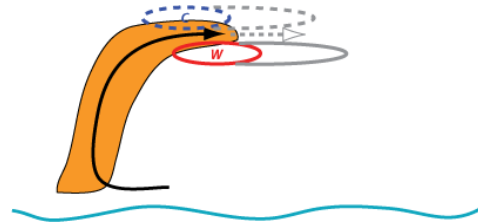


Fig. 11: Schematic model of anvil self-spreading due to radiative cooling and heating. See text.

Radiatively-induced anvil spreading. Fifteenth ARM Science Team Meeting Proceedings, Daytona Beach, Florida, March 14–18, 2005.

Rotunno, R. and K. A. Emanuel, 1987: An airsea interaction theory for tropical cyclones. Part II: Evolutionary study using a nonhydrostatic

- axisymmetric numerical model. *J. Atmos. Sci.*, **44**, 542–562.
- Shapiro, L. J. and H. E. Willoughby, 1982: The response of balanced hurricanes to local sources of heat and momentum. *J. Atmos. Sci.*, **39**, 378–394.
- Schubert, W. H. and J. J. Hack, 1982: Inertial stability and tropical cyclone development. *J. Atmos. Sci.*, **39**, 1687–1697.
- Seifert, A. and K. D. Beheng (2006): A two-moment cloud microphysics parameterization for mixed-phase clouds. Part I: Model Description. *Meteor. Atmos. Phys.*, **92**, 45–66.
- Wang, Y., 2009: How do outer spiral rainbands affect tropical cyclone structure and intensity? *J. Atmos. Sci.*, **66**, 1250–1273.
- Willoughby, H. E., 1979: Forced secondary circulations in hurricanes. *J. Geophys. Res.*, **84**, 317–3183.

*Acknowledgments.* This work was supported by NSF grant ATM-0554765 and the Jet Propulsion Laboratory SURP program. Computing facilities were provided by the Aerospace Corporation. Drs. Axel Seifert and Kuo-Nan Liou provided advice and feedback.